On-machine non-contact roughness verification system based on Conoscopic Holography

Pablo Zapico [a], Gonzalo Valiño [a,1], J. Carlos Rico [a], Víctor M. Meana [a], Pedro Fernández [a]

[a] Department of Construction and Manufacturing Engineering, University of Oviedo, Campus of Gijón, 33203 Gijón, Spain

[1] Corresponding author: *E-mail address:* gvr@uniovi.es (Gonzalo Valiño)

Abstract

The surface quality verification of mechanical components is an essential activity in many applications where surface performance plays an important role in the functional behaviour of the part. Although many of the verification techniques commonly employed are based on the use of contact roughness profilometers, there are some limitations related to the morphological filtering effect associated to the stylus tip radius, as well as the difficulty in using these type of styli to carry out on-machine surface verification. The use of non-contact digitizing techniques helps to overcome some of these drawbacks, although the verification of surface quality using these non-contact systems still requires the development of scanning and data processing procedures similar to those described in the international standards for contact probing techniques. This work analyses the use of a non-contact sensor, based on Conoscopic Holography and integrated in a 3-axis machining centre, applied to the verification of the surface roughness of parts machined by face and cylindrical milling processes. After the calibration of the integrated system, a high-frequency noise filtering procedure specifically designed for roughness verification is proposed. The results demonstrate the feasibility of the system for verifying surface roughness grades from N5 to N12 in the two milling processes. Finally, specific filtering recommendations for each roughness grade of both milling processes as well as a surface verification procedure are provided.

Keywords: Conoscopic Holography; Roughness; On-machine measurement; Non-contact measurement.

1. Introduction

Quality of mechanical parts is generally considered as a combination of dimensional and geometrical accuracy and a good surface finish. Among other properties, surface finish may affect component's fatigue and corrosion endurance, hardness and heat transfer capability [1-3], becoming an essential issue in the case of moulds, dies and mechanical implants. On the other hand, surface finish also affects interaction between different components working together in a mechanism, especially when a good fit and lubrication ought to be assured between two sliding surfaces to attenuate vibrations, wear and noise during their operation [4,5].

In the case of machined parts, it is well known that by adjusting the process parameters, different grades of surface roughness can be achieved [1,5,6]. Nevertheless, roughness verification becomes essential when high surface quality is required. Thus, the standard ISO 4287 defines how to evaluate surface quality by means of numerous roughness parameters associated to the surface topography [7]. Whereas there are surface evaluation methods based on visual and/or haptic perception by an operator, other quantitative methods based on instrumental measurements provide more objective and accurate approaches. Nowadays, many instrumental systems based on different technologies [2,4] (e.g., mechanical, optical, electrical, pneumatic, hydraulic, etc.) classified into contact or non-contact systems are used.

One of the most widespread contact method uses a stylus touch probe ended with a small-radius spherical tip (typically from 2 µm to 10 µm) that is slid on the surface to register

vertical fluctuations as the tip moves. Surface profiles are then extracted and several geometrical analysis and mathematical filtering is performed to calculate roughness parameters. Despite this technology is commonly used for reference measurements, it is not absent of drawbacks. Displacement of the stylus can cause damage to the measured surface, especially when using a diamond tip and testing a soft material [8]. Moreover, this contact measurement procedure in combination with the tip radius causes a morphological filtering effect on the digitized geometrical information of the profile [9]. Other weaknesses are the lack of accessibility to verify complex geometries (e.g., gearboxes or bearings [3,8]), a slow velocity of measurement [10] and the difficulty to automate the measurement process due to the need for precise movements and the high sensitivity to dirt [8,11].

The use of non-contact digitizing methods is more advantageous than contact ones, especially in automated procedures, where simpler movements are required and better accessibility is feasible, once any need for surface contact has been eliminated. Non-contact technologies may be classified into direct or indirect. Direct technologies are able to digitize the surface topography and extract the roughness parameters information. Optical profilers, non-optical microscopes, speckle methods, scattering methods, triangulation systems, etc., described in numerous publications, are common examples of direct technologies [12-15]. On the other hand, indirect methods do not digitize the surface topography but are able to state a correlation between information from different sensors and the value of the surface roughness parameters. In most cases, these methods are based on digital image processing [3,8,10,11] or acoustic sensors [16]. In terms of accuracy, direct methods are more suitable when surface roughness is a critical issue, due to the inability of indirect methods to manage possible unanticipated surface disturbances

(e.g., non-machining marks, chips, rests of cutting fluid, noise coupled to the sensor signals, etc.).

The aforementioned advantages provided by non-contact digitizing methods over contact ones have promoted the research and development of *in situ* non-contact roughness verification systems. In this sense, Quinsat and Tournier [2] present a non-contact STIL profilometer attached to the spindle of a 3-axis machine tool. Zou et al. [17] propose a low-coherence interferometer system coupled to an industrial robot for surface roughness verification of turbine blades. Another example by Sahabi and Ratnam [18] is a vision system integrated in a lathe for roughness measurement. Alternatively, He et al. [19] combine a fringe projection profilometer with a conoscopic holography sensor. Other numerous works develop non-contact roughness measurement systems in lab conditions although easy to integrate on production machines for on-machine verification activities. That is the case of confocal systems specifically developed [20], *ad-hoc* interferometric techniques [21] or different vision systems complemented with neural networks [1,8,11] or with other simpler math models [3,22]. Moreover, a great effort has been paid in the last years to develop on-machine non-contact digitizing systems focused on both digitizing and verification tasks [23-27].

Despite these works, even today non-contact surface roughness verification systems are not widely spread in industry maybe due to the lack of specific traceability standards, what forces developers to compare their results to those obtained with contact probes [11]. Another outstanding reason is the high influence of measurement conditions on the results achieved, such as the optical surface behaviour, the distance location of the sensor with respect to the surface [24,28-31] or the nature of the non-contact technology used. Therefore, a major effort still needs to be made for the characterisation of each technology in order to obtain sufficiently reliable roughness measurements.

Taking into account the above considerations, this work presents an on-machine non-contact roughness surface verification system based on Conoscopic Holography (CH) [32]. This incoherent light interferometric technique based on birefringent properties of crystals can be used in relatively compact sensors ease to integrate in production machines [33]. These sensors developed by Optimet have been used to demonstrate the applicability of CH for different non-contact measurement and digitizing tasks in varied fields, such as metrology and process control [34-37], art [38], medicine [39], forensic techniques [40,41], etc. In this work, a ConoPoint-10 CH sensor by Optimet was integrated in a 3-axis machining centre (MC). After both intrinsic and extrinsic calibration procedures were performed to set correlations between the sensor measurements and the MC coordinate system, different surface roughness gauges corresponding to both face and cylindrical milling processes were digitized using the on-machine integrated sensor. The values of roughness parameters Ra and Rz extracted from the digitized information were compared to those values delivered by the gauges' manufacturer. CH-dependent specific filtering recommendations are provided for each roughness grade on both milling processes, adapted from guidelines stated within international roughness standards referred to contact profilometers. As a result, Conoscopic Holography is demonstrated as an effective on-machine non-contact technology feasible to provide reliable roughness measurements in industrial milling processes.

Table 1 Characteristics of the ConoPoint-10 CH sensor [42]

Characteristic	Lens 16 mm
Working frequency, F (Hz)	up to 9000
Power level, P (1) (%)	0 – 100
Depth of Field, DOF (mm)	0.6
Stand-off (mm)	9.5
Laser wavelength (nm)	655
Linearity (2) ±%	0.33
Laser spot size (FWHM) w (3) (μm)	20
Repeatability (static) (4) (μm)	0.06
Reproducibility (dynamic) (5) (μm)	0.15

Angular coverage (°)	150

(1) Maximum power level is equivalent to 1 mW

(2) Maximum deviation between measurement and its nominal distance over the measurement range.

(3) Spot size is the effective width for measurement that contains 50% of the energy delivered, as measured at the centre of the working range.

(4) Standard Deviation of 10000 static measurements of a flat surface.

(5) Average of standard deviation between two flat surfaces measured 50 times.

2. On-machine digitizing system

The work described in this study was performed using a ConoPoint-10 CH point sensor by Optimet. The sensor visible light source is a Class II laser diode of 655 nm wavelength. A lens of 16 mm focal length and 0.6 mm depth of field (DOF) was coupled to the sensor. Each sensor's reading provides the value of distance between the sensor and the laser spot projected on the material surface. Table 1 shows the main characteristics of the CH sensor [42].

The sensor was integrated in a 3-axis MC Lagun Lean L1000 equipped with a FANUC M0i controller. This is a kind of vertical spindle MC with horizontal table movement (X,Y) and vertical head movement (Z). All the axes are equipped with linear incremental encoders with 1 μm resolution.

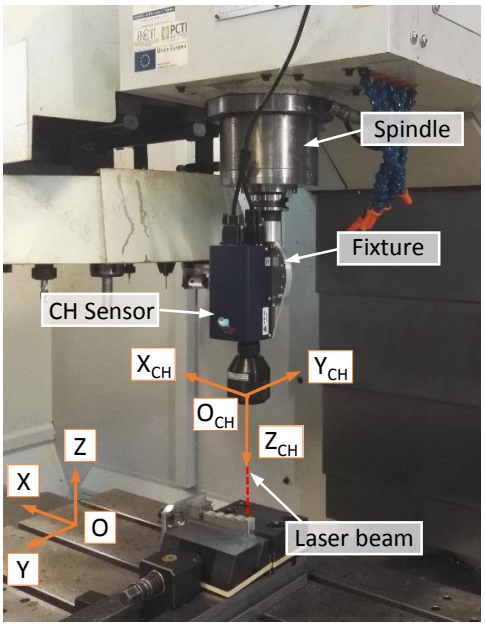

Fig. 1 CH sensor held in the MC spindle and characteristic coordinate systems

The CH sensor is held in the MC spindle by means of a tailor-made adaptor fixed on a standard cone (DIN 69871), similar to that of any other tool (Fig. 1). It is possible to move the sensor three-dimensionally so that the distance remains constant over the whole surface to be digitized and coincident with the stand-off characteristic value of the lens. This way, all the points shall be acquired within the lens DOF.

With the aim to achieve coordinated operation between the CH sensor and the MC, an ad-hoc application was developed using the software development kits (SDK) provided by their respective manufacturers. This application runs on a PC connected via Ethernet with both devices and allows for moving the MC axes to a target position and then performing the measurements with the CH sensor. Since the CH sensor interface was connected to the linear encoders of the MC axes, each sensor's measurement was related to a reading of the linear encoder during the continuous movement of the MC axes. Thus, high density digitizing is achieved up to 250 measurements/mm at a maximum feedrate of 2160 mm/min. This operating conditions make it possible to capture point clouds detailed enough to analyse the topography of surfaces.

Prior to perform any measurement, the CH sensor operating parameters (power level and working frequency) must be adjusted based on two signal quality indicators (Signal-to-Noise Ratio (SNR) and Total) related to the optical behaviour of the surface [43]. The Power Level sets the laser power emitted by the sensor while the Working Frequency establishes the measurement capturing rate. According to manufacturer's recommendations accurate measurements will be achieved for SNR higher than 50% and Total within the range 1200 to 21000 [42].

This set-up procedure is performed via a graphical interface (GUI) that allows the user to adjust the working distance, the operating parameters and check the quality indicators in real time by means of a graphical representation of the signal detected on the sensor CCD.

2.1 System calibration

The ConoPoint-10 CH sensor provides the distance between a reference plane and a point on a surface, by the analysis of the reflected incoherent light, using the double refraction property of birefringent crystals. For this purpose, the sensor's CCD detects the frequency of an interference pattern generated by the laser light previously emitted by the sensor and reflected by the surface [44]. The use of lenses with different DOF enables to adapt this sensor to different measurement precision requirements. This requires that each lens be intrinsically calibrated for the sensor, so that when switching from one lens to another, the sensor can be quickly reconfigured by software to adapt the interference pattern analysis to the current lens coupled to the sensor.

In this work, a lens of 16 mm focal length was chosen for surface quality verification and an intrinsic calibration procedure had to be performed since it was a new lens not previously calibrated. To carry out the intrinsic calibration procedure, the tailor-made fixture set-up shown in Fig. 2 was used. As it can be seen, the CH sensor was fixed on the MC table so that the laser beam was aligned with X direction. On the other hand, a

test part with good optical surface properties was held in the spindle and oriented perpendicular to the laser beam.

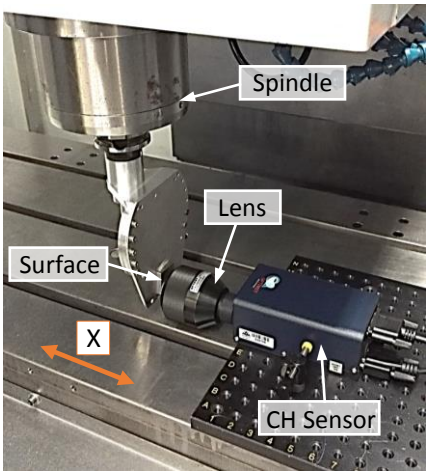

Fig. 2 Tailor-made fixture set-up for lens intrinsic calibration

The intrinsic calibration procedure consisted in measuring 500 positions distributed every 2 µm along 1 mm on the X axis. Using an acquisition rate of 3000 Hz, 1500 measurements were taken at each position and the average frequency of the interference pattern detected on the CCD was calculated so that a relationship was obtained between this frequency (f) and the relative surface-sensor distance (γ). This relationship was fitted by means of the fourth degree polynomial expressed in Eq. (1), whose coefficients are presented in Table 2.

$$\hat{\gamma}(f) = a_4 \cdot f^4 + a_3 \cdot f^3 + a_2 \cdot f^2 + a_1 \cdot f + a_0 \text{ [mm], being f in Hz} \qquad (1)$$

Table 2 Coefficients of the polynomial used for intrinsic calibration

Coefficient	Value
a_4	$-5.22809 \cdot 10^{-14}$
a_3	$3.26715 \cdot 10^{-10}$
a_2	$-1.00340 \cdot 10^{-6}$
a_1	$1.98459 \cdot 10^{-3}$
a_0	8.47426

The results from the fitted polynomial for different positions compared to the actual MC X axis positions are represented in Fig. 3.

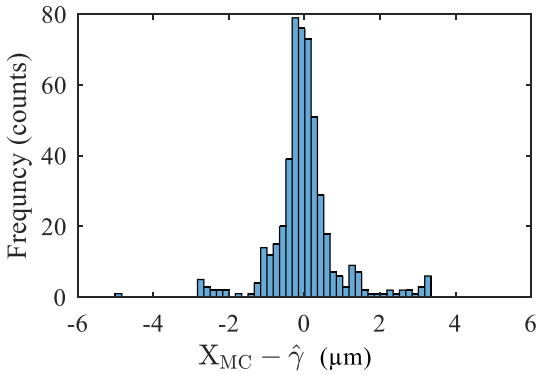

Fig. 3 Fitting error of the fourth degree polynomial used for intrinsic calibration

Once performed the intrinsic calibration, the measurements taken by the sensor are related to the sensor's internal coordinate system. In order to express these measurements with respect to the MC coordinate system, extrinsic calibration of the sensor integrated in the MC has to be carried out. As it can be seen in Fig. 4a, extrinsic calibration might be achieved by means of the following vector expression:

$$\mathbf{P}_{\mathrm{i}} = \mathbf{P}_{\mathrm{Q}_i} + \mathbf{t} + \gamma_{\mathrm{i}} \cdot \mathbf{a} \qquad (2)$$

where $\mathbf{P}_{\mathrm{Q}_i}$ represents the position vector of the spindle nose with respect to the MC origin. Vector **t** represents the offset of the CH reference system origin with respect to the MC spindle and **a** is a unit vector aligned with the measuring direction of the sensor. Multiplying this vector by the measure γ captured by the CH sensor, the vector that links the sensor reference system origin with the measured point is obtained.

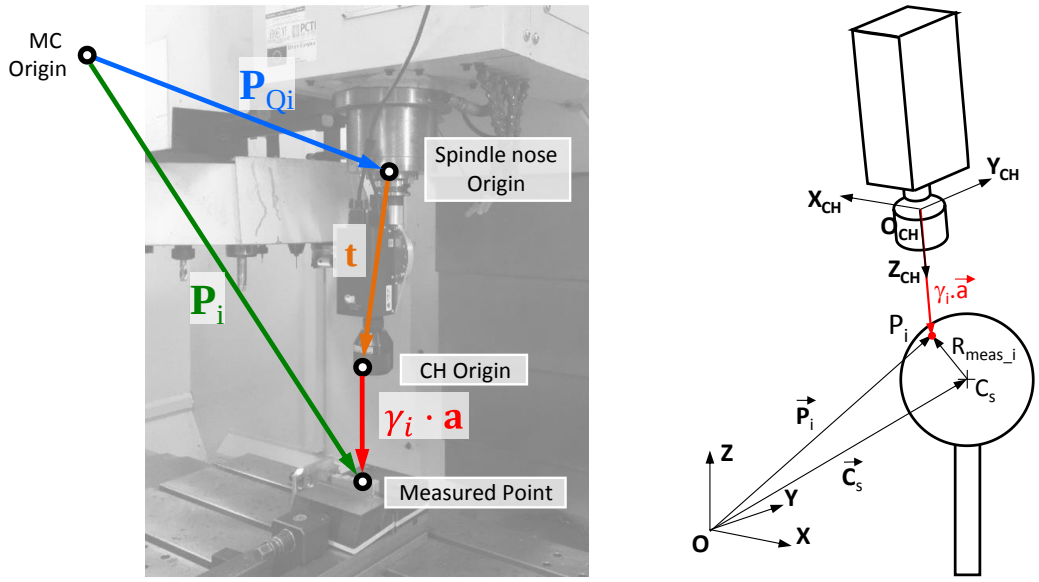

(a) (b)

Fig. 4 (a) Vectors for extrinsic calibration of the integrated CH sensor, (b) relationship between a measured point P_i and the centre C_s of a test sphere

In Eq. (2), the spindle nose position $\mathbf{P}_{Q_i}$ at each point is always known by the CNC controller and distance γ_i is measured by the CH sensor. The vectors **a** and **t** shall be determined by means of indirect methods, by digitizing a set of points which keep a known geometrical relationship among them. For this, the set of points is taken on the surface of an artefact of known dimensions.

In this work, a calibrated sphere was used as the artefact, whose centre position and radius were known (Fig. 4b). The centre of the sphere C_s was determined by means of the contact probe (Renishaw OMP 400) available in the MC. In this case, the value of radius R_s was extracted from the calibration certificate (6.326 mm). A relatively small sphere was used in order to digitize a sufficient area with the sensor, considering the small DOF of the 16 mm lens. A collection of 12000 points were digitized by means of the CH sensor following a 3D spiral on the upper half of the sphere and covering a cone angle of 90°, so that all the points laid within the lens DOF.

According to the geometrical relationship shown in Fig. 4b, the sphere radius (R_{meas_i}) at the point digitized by the CH sensor may be calculated as:

$$R_{meas\_i} = |\mathbf{P}_i - \mathbf{C}_s| \quad (3)$$

Since the real sphere radius (R_s) is known, the measurement error at each point can be expressed as follows:

$$\delta_i = R_{meas\_i} - R_s \quad (4)$$

Joining Eq. (3) and Eq. (4), the measurement error becomes:

$$\delta_i = |\mathbf{P}_i - \mathbf{C}_s| - R_s \quad (5)$$

In order to determine the vectors **a** and **t** with precision, the errors δ_i should be reduced for all the points simultaneously. The process is carried out by minimizing the following non-linear function by the Gauss-Newton iterative method:

$$f = \sum_{i=1}^{n} \delta_i^2 \quad (6)$$

where n represents the number of digitized points.

3. Materials and methods

3.1 Roughness gauges

To analyse the roughness measurement performance of the CH sensor, face and cylindrical milling roughness gauges Rugotest (TESA©) and Microsurf (Rubert & CO. LTD.) were used. Table 3 shows the roughness grades measured and their associated parameters, according to ISO 1302.

Table 3 Values of roughness parameters of face and cylindrical milling roughness gauges

	Face milling roughness grade							
	N5	N6	N7	N8	N9	N10	N11	N12
Ra (µm)	0.4	0.8	1.6	3.2	6.3	12.5		
Rz (µm)	2	4	8	16	32	63		
	Cylindrical milling roughness grade							
	N5	N6	N7	N8	N9	N10	N11	N12
Ra (µm)	0.4	0.8	1.6	3.2	6.3	12.5	25	50
Rz (µm)	1.80	3.68	6.63	12.8	25.6	53	97.5	197

3.2 Digitizing of roughness gauges

Each roughness grade of the gauges was digitized by means of the CH sensor integrated in the MC following a continuous zig-zag scanning strategy that covers a rectangular area of 18 mm x 4 mm. Points were taken every 4 µm along each pass and an inter-pass distance of 75 µm was used. Thus, about 240000 points were captured in each point cloud.

The adjustment of the CH sensor was set to pulse-trigger mode, in order to perform continuous scanning, using a frequency of 3000 Hz and 100% of laser power. Additionally, auto-exposure mode was enabled to achieve enough digitizing quality regardless the shine and the scattering of reflected light typical of machined surfaces [45-46]. Once the digitizing processes were performed for each of the roughness grades, both intrinsic and extrinsic calibrations were applied to express the point clouds referred to the MC coordinate system. These point clouds were processed applying a wide threshold outlier filter (±10 σ) to remove inconsistent measurements (less than 0.02%). The point clouds were then converted into regular arrays of Z-values on the XY axes by linear interpolation in order to enable the extraction of roughness profiles in the desired directions. The processed point clouds for the N10 roughness grade of face and cylindrical milling gauges are shown in Fig. 5.

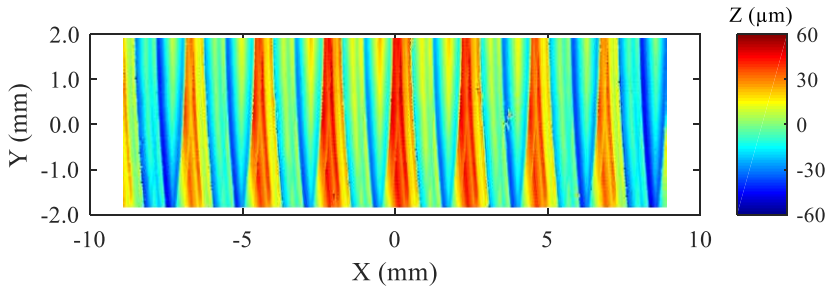

(a)

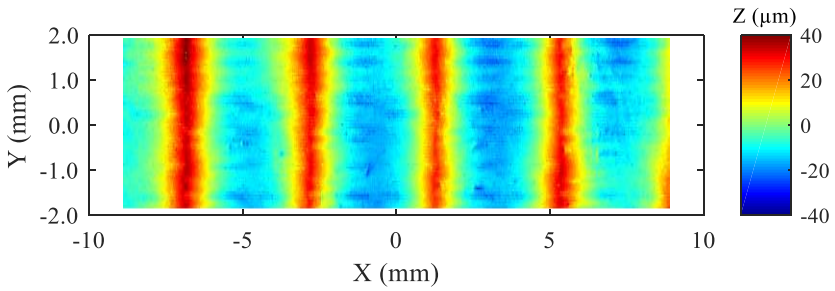

(b)

Fig. 5 N10 roughness grade processed point clouds: (a) face milling, (b) cylindrical milling

3.3 Processing of roughness profiles

Roughness profiles are extracted from the point clouds to determine parameters Ra and Rz, as the example shown in Fig. 6.

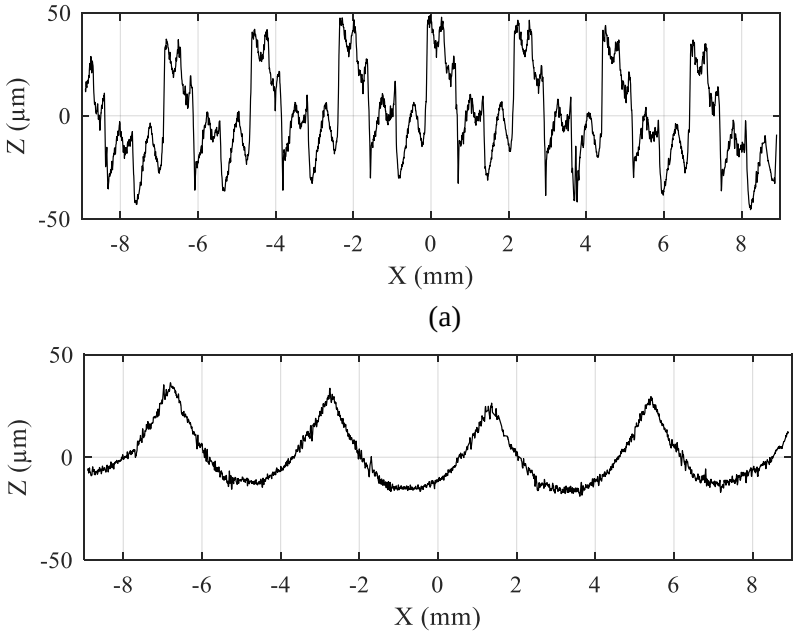

(a)

(b)

Fig. 6 Roughness grade N10 extracted centre profile: (a) face milling, (b) cylindrical milling

According to standard ISO 4288 [47], these extracted profiles must be processed using a combination of low-pass (LP) and high-pass (HP) Gaussian filters. These two filters constitute a band-pass filter referred as filter bank in ISO 16610-20 [48]. The HP filter removes long wavelength (low frequency) components of the roughness profile whereas

the LP filter removes short wavelength (high frequency). This way, both waviness and high frequency noise are removed from the original profile and makes it possible to analyse surface roughness. According to ISO 4288, λ_c and λ_s represent the cut-off values to define the HP and LP filters, respectively (Fig. 7).

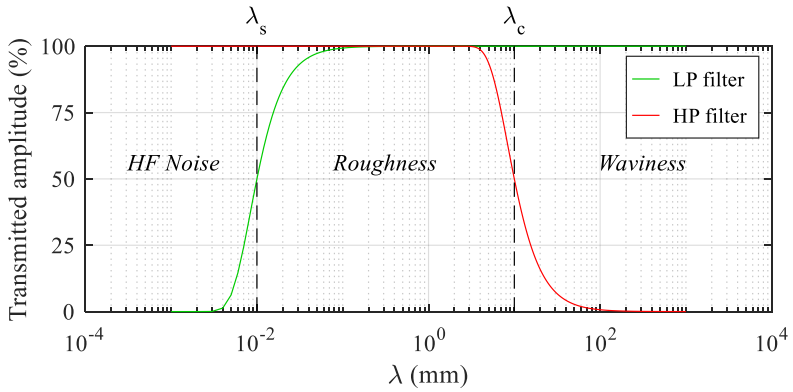

Fig. 7 Filtering procedure to extract roughness profile (ISO 4288)

As described in ISO 16610-21 [49], the application of these Gaussian filters consists in processing the profile data with a convolution whose kernel is the weighting function defined in Eq. (7):

$$s(x) = \frac{1}{\alpha\lambda} \exp\left[-\pi\left(\frac{x}{\alpha\lambda}\right)^2\right] \tag{7}$$

where x represents the distance between the location filtered and the rest of the profile points, λ the cut-off value of the filter and α is a constant whose value ($\sqrt{\ln 2}/\sqrt{\pi}$) ensures a 50% of amplitude transmission for a component with a wavelength equal to the cut-off length. Thus, the amplitude of the weighting function depends on the cut-off value. It can be noticed also in Eq. (8) that there is a relationship between the cut-off and the standard deviation σ that defines the amplitude of the Gaussian kernel function. This kernel must be applied at each position of the captured profile covering its neighbourhood. According to ISO 16610, a unitary truncating value, e.g. neighbourhood of $x \pm \lambda$, ensures an implementation error lower than 10^{-5} %.

$$\sigma = \frac{\alpha}{\sqrt{2\pi}} \cdot \lambda = \frac{\sqrt{\ln 2}}{\pi \cdot \sqrt{2}} \cdot \lambda \quad (8)$$

The setting of the cut-off values of this band-pass filter depends on the characteristics of the surface to be analysed.

Table 4 Sampling length and evaluation length values corresponding to RSm according to ISO 4288

RSm (mm)	Sampling length l_r (mm)	Evaluation length l_n (mm)
$0.013 < RSm \leq 0.04$	0.08	0.4
$0.04 < RSm \leq 0.13$	0.25	1.25
$0.13 < RSm \leq 0.4$	0.8	4
$0.4 < RSm \leq 1.3$	2.5	12.5
$1.3 < RSm \leq 4$	8	40

In the case of periodical surface profiles such as those obtained by machining processes (e.g., turning or milling), the low frequency filter is set with a cut-off wavelength (λ_c) which depends on the mean value of the roughness profile elements width (RSm) within an evaluation length (l_n). Following ISO 4288 recommendations, this evaluation length is composed of five sampling lengths (l_r), whose lengths coincides with λ_c. Therefore, it is necessary to perform a preliminary test before analysing the roughness to measure the RSm value to determine the cut-off value of this filter from Table 4. The results of these preliminary tests and the corresponding λ_c values obtained for each process and roughness grade analysed are shown in Table 5.

Table 5 Face Milling and Cylindrical Milling RSm and corresponding l_r and λ_c values

	Face milling roughness grade							
	N5	N6	N7	N8	N9	N10	N11	N12
RSm (mm)	0.28	0.33	0.36	0.50	1.35	2.25		
l_r, λ_c (mm)	0.8	0.8	0.8	2.5	8.0	8.0		
	Cylindrical milling roughness grade							
	N5	N6	N7	N8	N9	N10	N11	N12

RSm (mm)	0.33	0.35	1.61	2.06	2.41	4.11	6.37	10.9
l_r, λ_c (mm)	0.8	0.8	8.0	8.0	8.0	-	-	-

As it can be noticed, no λ_c values were assigned to N10 to N12 cylindrical milling roughness grades since the RSm values measured for them were outside the ranges included in Table 4. Thus, no low frequency filtering was applied to these grades.

As an application of this waviness filtering procedure to the N8 face milling gauge, the original roughness profile, the waviness profile and the resulting waviness filtered profile (i.e. the HP filtered component) are shown in Fig. 8.

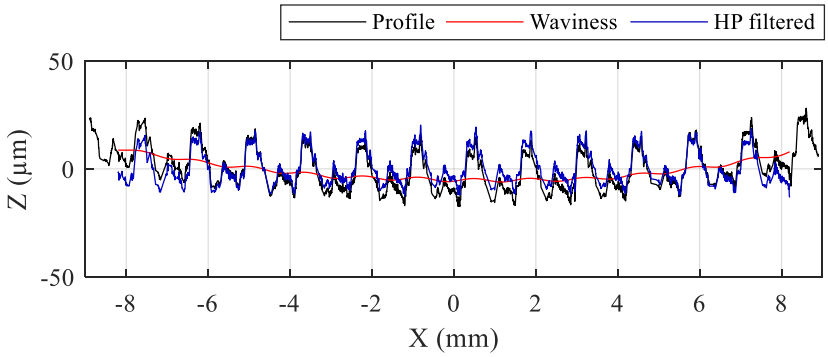

Fig. 8 Low frequency filtering of a face milled N8 profile ($\lambda_c = 2.5$ mm, ISO 4288)

Once the low frequency filter to be applied has been specified, the cut-off value of the high frequency filter must be set. In this case, the cut-off wavelength (λ_s) used is lower than the one in the case of the low frequency filter (λ_c). ISO 3274 [50] states relationships of λ_c/λ_s within the range 30 to 300 for contact profilometers.

As an example, Fig. 9 shows the application of low and high frequency filters to a roughness profile corresponding to grade N8 of the face milling gauge, using two different values of the ratio λ_c/λ_s. With the Fast Fourier Transforms shown in Fig. 10, it can be noticed that the ratio $\lambda_c/\lambda_s = 30$ leads to a higher attenuation of high frequency

noise than in the case that $\lambda_c/\lambda_s = 300$ and, in turn, a smoother filtered profile is achieved.

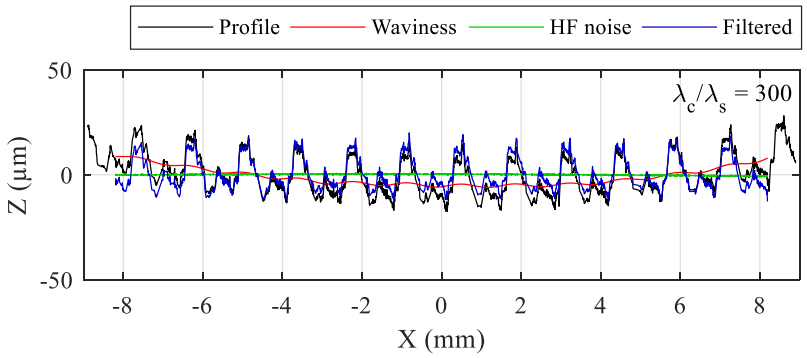

(a)

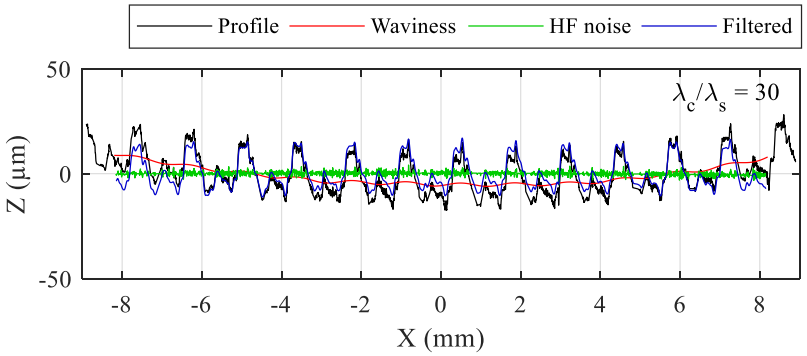

(b)

Fig. 9 Low and high frequency filters applied to N8 roughness grade in face milling: (a) $\lambda_c = 2.5$ mm, $\lambda_s = \lambda_c/300$, (b) $\lambda_c = 2.5$ mm, $\lambda_s = \lambda_c/30$

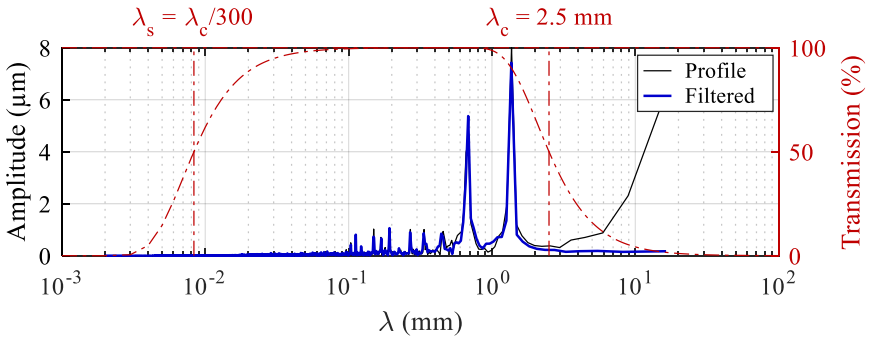

(a)

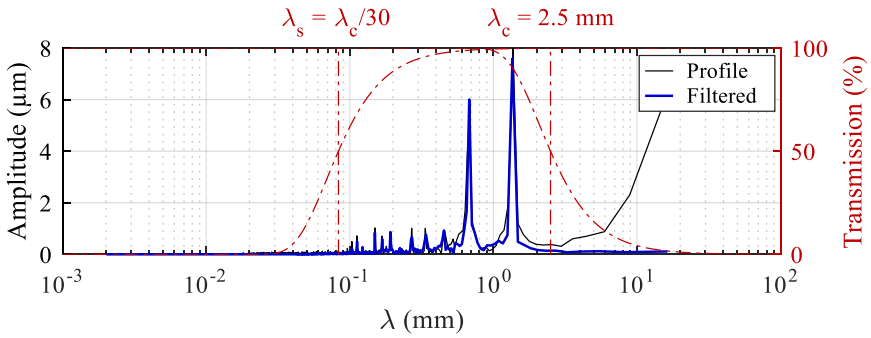

(b)

Fig. 10 Fast Fourier Transforms of low and high frequency filters applied to N8 roughness grade in face milling: (a) $\lambda_c = 2.5$ mm, $\lambda_s = \lambda_c/300$, (b) $\lambda_c = 2.5$ mm, $\lambda_s = \lambda_c/30$

As already mentioned, the recommendations of ISO 3274 refer to contact profilometers. Among other things, this standard addresses the morphological filtering effect associated with the stylus tip radius or the stability of static measurements. In the case of non-contact profilometers, as the CH sensor used in this work, some recommendations of the ISO 3274 standard should not be applied, being necessary to develop specific recommendations based on their own non-contact measurement nature.

In the case of the CH technology, lens used is one of the most influencing factors on measurements quality, characterized by the depth of field (DOF) and the spot size. Depending on the chosen lens, different conditions of static measurement repeatability, angular coverage or lateral resolution may be achieved. It is also assumed that the smaller the DOF, the better the measurement performance. On the other hand, similarly to other optical technologies, the measurement performance of CH sensors is also affected by external factors as the optical properties of the digitized surface. Therefore, recommendations for roughness measurement with CH technology should consider both internal and external factors.

Two of the main internal factors to consider in CH sensors are the size and shape of the laser spot. Laser spot shows an asymmetry that affects the lateral resolution of digitizing

along the two normal directions and, in order to meet a similar performance to other non-contact systems considered as reference, Gaussian-type filters related to the spot geometry must be applied to attenuate high frequency noise coupled to the CH digitizing data [51].

With the aim to improve the high resolution digitizing performance of a CH sensor, a Gaussian filter related to the laser spot size (w) was established by Patiño et al. [51], using a confocal microscope as the reference digitizing instrument.

The CH spot size (w) is defined as the Full Width at Half Medium (FWHM) of the spot at the standoff position within the DOF. This means that, in such a position of the DOF, 50% of the spot light intensity is concentrated within this spot dimension. According to this definition and considering that the laser spot light intensity on the surface is normally distributed, the FWHM can be obtained as in Eq. (9), where σ represents the standard deviation of the spot light intensity.

$$\text{FWHM} = w = 2 \cdot \sqrt{2 \cdot \ln 2} \cdot \sigma \tag{9}$$

Considering Eq. (8) and Eq. (9) together, the cut-off wavelength related to the laser spot size can be obtained as follows:

$$\lambda_s = \frac{\pi \cdot w}{2 \cdot ln\, 2} \tag{10}$$

As it was mentioned, this relationship must be tuned to improve measurement performance. Thus, a gain parameter k was included to adjust the Gaussian kernel size, (i.e., Gaussian cut-off value) as follows:

$$\lambda_s = \frac{\pi \cdot w}{2 \cdot ln\, 2} \cdot k \tag{11}$$

The measurement recommendations by using this tuning procedure result quite similar to those found in ISO 4288 [47] for contact profilometers. These instruments are dependent

on both the roughness grade measured and the type of process used to manufacture the surface, e.g. whether they are periodical or non-periodical roughness profiles. Then, recommendations in ISO 4288 for contact profilometers can be applied to the CH sensor by using a proper tuning procedure.

In this research the filtering procedure proposed for CH sensors affects more importantly in those cases where the amplitude of noise coupled to the digitized data is closer to the amplitude of the roughness component. Due to its high frequency filtering nature, a similar situation occurs in the case of contact profilometers. Thus, the application of this procedure becomes practically mandatory in the case of fine roughness grades (lower than N8) whereas it becomes accessory for coarser ones.

4. Results and discussion

In order to obtain reliable values of the roughness parameters Ra and Rz, ten profiles were analysed on each roughness gauge, extracted from the point clouds gathered with the CH sensor (section 3.2). These profiles were initially processed with a low frequency filter to remove waviness and then, noise attenuation was carried out by applying a high frequency filter under several values of the gain parameter *k*. Next, average values of Ra and Rz were obtained for each case.

With regard to the face milling gauge, Fig. 11 shows deviations of the roughness parameters with respect to the gauges nominal values under different values of k. A reasonable $\pm 10\%$ interval of deviation (target interval) is also represented.

When the high frequency filter is not applied ($k = 0$), deviations of Ra lay within the target interval in the cases of N8 and N9 whereas these deviations are remarkable for the rest of the roughness grades (Fig. 11a). In the case of the finest grades (N5 to N7), this occurs because the high frequency noise coupled to the digitized data has similar

wavelength to that of the roughness component. In those cases, it is necessary to apply the high frequency filter to meet deviations of Ra within the target interval, so that each roughness grade may require a different value of k for this purpose. In this way, values of $k = 1.0$, $k = 1.9$ and $k = 0.3$ are recommended for grades N5, N6 and N7, respectively.

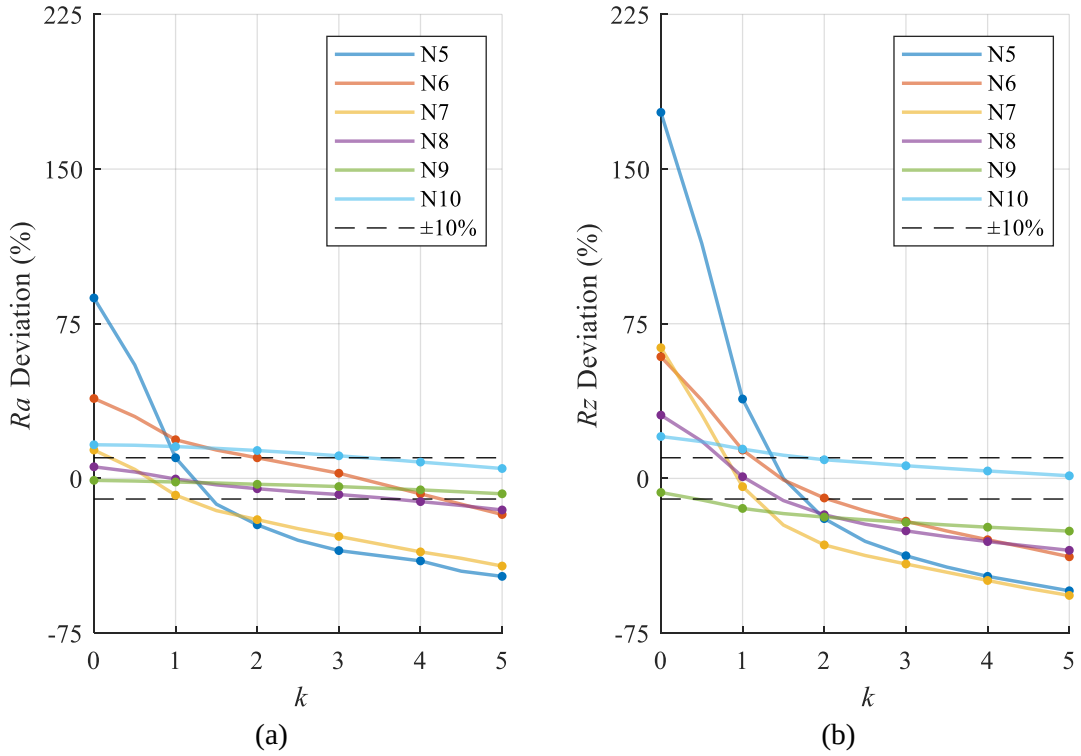

Fig. 11 Deviations of Ra and Rz with respect to the gauges nominal values under different values of k in face milling: (a) Ra deviations, (b) Rz deviations

Something similar occurs with deviations of Rz. As it can be observed in Fig. 11b, most of the roughness grades show notable deviations with regard to the reference values when the high frequency filter is not applied ($k = 0$). Therefore, high frequency filtering is mandatory in the cases N5 to N8 to keep deviations within the target interval. Values of $k = 1.4$, $k = 1.2$ are suggested for grades N5 and N6, respectively, and $k = 0.8$ for N7 and N8.

Regarding grade N10, both parameters Ra and Rz present a curious behaviour since they have to be filtered with values of *k* greater than those of finer grades (e.g., N9). This may be due to differences between the filters used by the gauges' manufacturer and the ones recommended in ISO 4288 [47]. In order to verify this suspect, a contact profilometer was used to measure the gauge N10 considering ISO 4288 recommendations ($\lambda_c = 8$ mm and $\lambda_s = 25$ µm). Values of $Ra = 14.09$ µm and $Rz = 74.45$ µm were obtained which were higher than the values provided by the manufacturer ($Ra = 12.5$ µm and $Rz = 63$ µm) (Table 3).

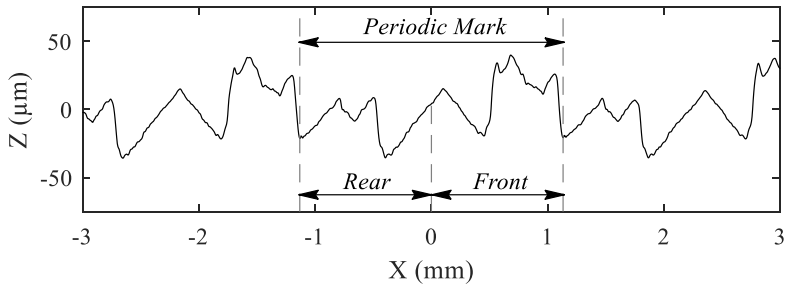

Fig. 12 Roughness grade N10 measured with a contact profilometer on the face milling roughness gauge

To understand this discrepancy, the measured roughness profile corresponding to grade N10 was analysed graphically as shown in Fig. 12. It can be noticed that the periodic mark related to the milling feedrate used initially to obtain the RSm value according to Table 5 ($RSm = 2.25$ mm) can be understood as the contribution of both the front and the rear passes of the mill. Thus, the calculus of RSm should consider either the front or the rear contributions (approximately 1 mm each one), but not both together. Then, taking $RSm \approx 1$ mm and the corresponding recommended values of $\lambda_c = 2.5$ mm (Table 4) and $\lambda_s = 8$ µm (ISO 3274), the roughness parameters measured by the contact profilometer on the N10 gauge were $Ra = 12.86$ µm and $Rz = 61.60$ µm, much closer to those values provided by the manufacturer. Using the latter filtering parameters, updated graphs of deviations of Ra and Rz were represented in Fig. 13 where now it can

be observed that, in the case of grade N10, they lay within the target interval. Therefore, $\lambda_c = 2.5$ mm and $\lambda_s = 8$ µm is the filtering configuration proposed and used in this work to analyse the N10 roughness grade, matching with the information provided by the gauges' manufacturer.

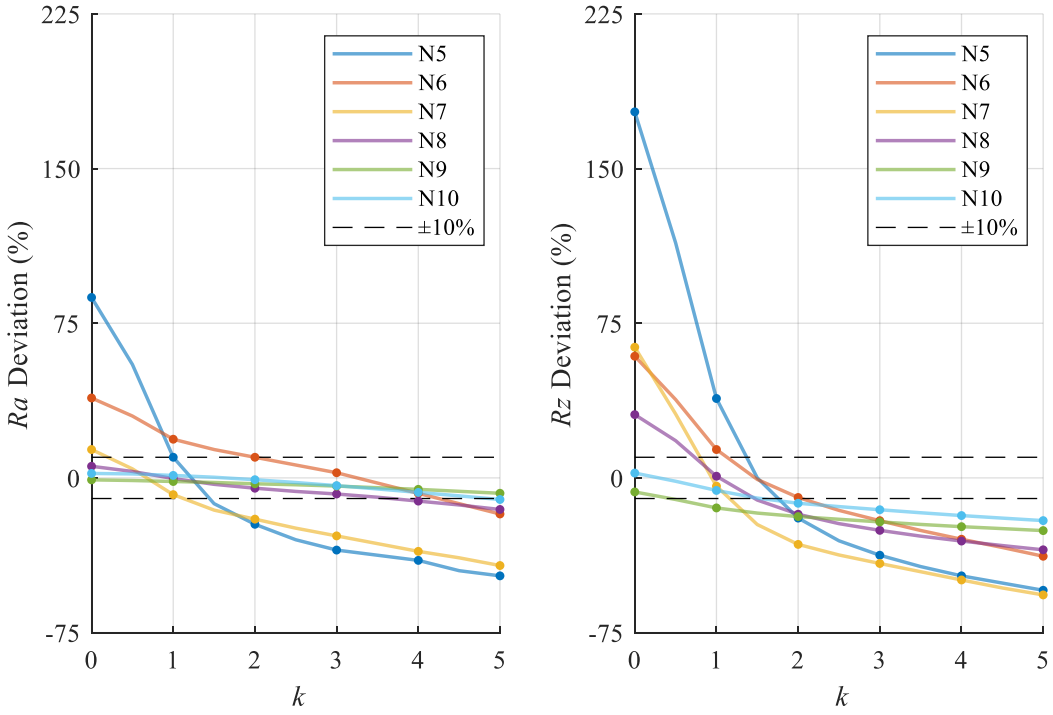

(a) (b)

Fig. 13 Deviations of Ra and Rz with respect to the gauges nominal values under different values of k in face milling, using $\lambda_c = 2.5$ mm and $\lambda_s = 8\ \mu$m for N10. (a) Ra deviations, (b) Rz deviations

The summary of deviations of Ra and Rz are included in Table 6 corresponding to each roughness grade in face milling. On the one hand, deviations obtained without applying a high frequency filter ($k = 0$) are provided. On the other hand, they are also included the gain values k for which deviations fall within the target interval as well as the values of k for which the lowest deviations are met in each case.

Table 6 Deviations of Ra and Rz in face milling. Effect of applying different high frequency filters

No HF Filtering	HF Filtering ($k \neq 0$)	
($k = 0$)	Within target interval ±10%	Minimum deviation ($k \leq 5$)

	Grade	Deviation (%)	k	λ_c/λ_s	Deviation (%)	k	λ_c/λ_s	Deviation (%)
Ra	N5	87.5	1.0	17.7	10.0	1.2	14.7	0.0
	N6	38.8	1.9	9.3	10.0	3.2	5.5	0.0
	N7	13.7	0.3	58.8	10.0	0.6	29.4	1.3
	N8	5.6	0.0	-	5.6	0.9	61.3	0.0
	N9	- 1.0	0.0	-	- 1.0	0.0	0.0	- 1.0
	N10	2.2	0.0	-	2.2	1.6	34.5	0.1
Rz	N5	177.5	1.4	12.6	4.5	1.5	11.8	0.0
	N6	59.0	1.2	14.7	7.3	1.5	11.8	- 0.7
	N7	63.4	0.8	22.1	7.6	0.9	19.6	0.9
	N8	30.7	0.8	68.9	7.1	1.0	55.2	0.8
	N9	- 6.8	0.0	-	- 6.8	0.0	-	- 6.8
	N10	2.3	0.0	-	2.3	0.4	137.9	- 0.3

A similar analysis was performed regarding cylindrical milling. Deviations of Ra and Rz with respect to manufacturer's values (Table 3) under different high frequency filtering gain values (k) are represented in Fig. 14. As in the case of face milling, λ_c was also set according to ISO recommendations (Tables 4 and 5).

Once again, it is necessary to apply high frequency filters to the finer grades for the roughness parameters Ra and Rz to become similar to those provided by the gauges' manufacturer. Thus, values of $k = 2.6$ and $k = 2.3$ are required for N5 and N6 and $k = 0.3$ for N8 in order for the deviation of Ra to fall within the target interval (Fig. 14a). Regarding deviation of Rz (Fig. 14b), a greater number of roughness grades require high frequency filtering since this parameter is more sensitive to noise. In this way, values of $k = 3.5$, $k = 2.7$, $k = 1.9$ and $k = 2.0$ ought to be applied to grades N5, N6, N7 and N8, respectively. On the other hand, as aforementioned in section 3.3, no λ_c values can be obtained for roughness grades N10 to N12 so that no waviness filtering could be applied to those grades. A summary of the results obtained for roughness processing in cylindrical milling is shown in Table 7.

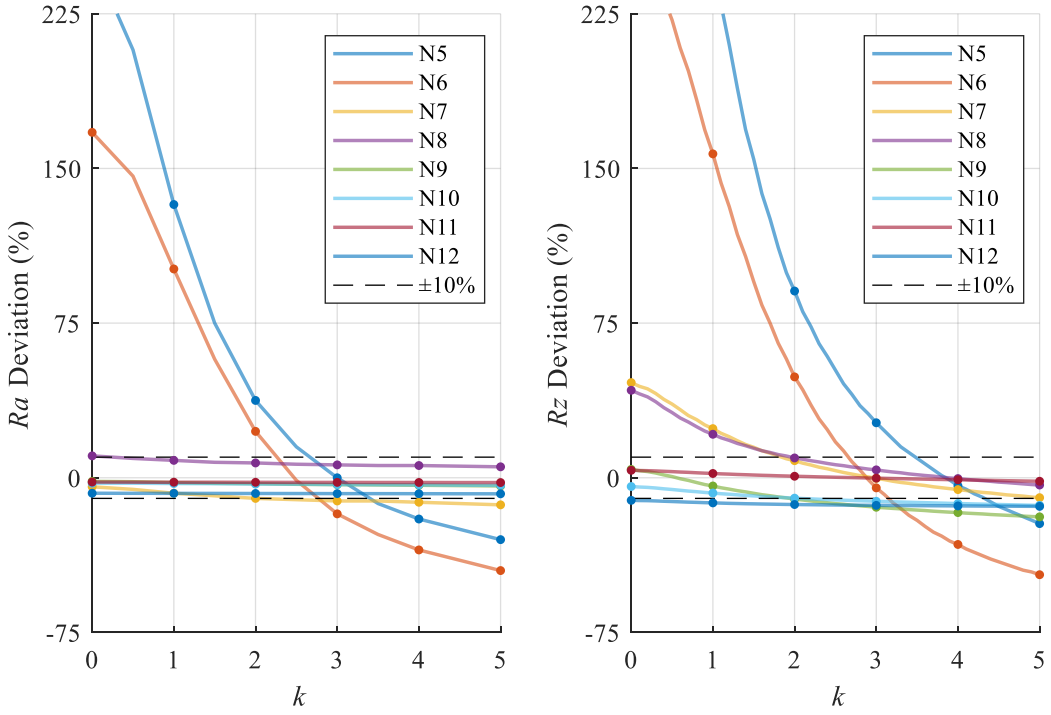

(a) (b)

Fig. 14 Deviations of roughness parameters with respect to the gauges nominal values under different values of k in cylindrical milling. (a) Ra deviations, (b) Rz deviations

Table 7 Deviations of Ra and Rz in cylindrical milling. Effect of applying different high frequency filters

		No HF Filtering ($k = 0$)	HF Filtering ($k \neq 0$)					
			Within target interval ±10%			Minimum deviation ($k \leq 5$)		
	Grade	Deviation (%)	k	λ_c/λ_s	Deviation (%)	k	λ_c/λ_s	Deviation (%)
Ra	N5	252.5	2.6	6.8	10.0	3.0	5.9	0
	N6	167.5	2.3	7.7	6.2	2.5	7.1	- 1.3
	N7	- 4.4	0.0	-	- 4.4	0.0	-	- 4.4
	N8	10.6	0.3	588.4	10.0	4.8	36.8	5.3
	N9	- 1.7	0.0	-	- 1.7	0.0	-	- 1.7
	N10	- 2.6	0.0	-	- 2.6	0.0	-	- 2.6
	N11	- 2.1	0.0	-	- 2.1	0.0	-	- 2.1
	N12	- 7.5	0.0	-	- 7.5	0.0	-	- 7.5
Rz	N5	469.4	3.5	5.0	9.4	3.8	4.6	1.1
	N6	262.5	2.7	6.5	7.9	2.9	6.1	- 0.8
	N7	46.2	1.9	92.9	9.2	3.0	58.8	- 0.3
	N8	42.4	2.0	88.3	9.6	3.9	45.3	- 0.1
	N9	4.1	0.0	-	4.1	0.6	294.2	- 0.5
	N10	- 4.2	0.0	-	- 4.2	0.0	-	- 4.2
	N11	3.6	0.0	-	3.6	2.8	-	0.0
	N12	- 10.9	0.0	-	- 10.9	0.0	-	- 10.9

5. Conclusions

An on-machine roughness non-contact verification system based on Conoscopic Holography integrated in a 3-axis MC is described in this work.

Both intrinsic and extrinsic calibration procedures were performed to state correlations between the sensor measurements and the MC coordinate system, becoming possible in this manner to carry out on-machine surface digitizing with enough accuracy for a later roughness analysis.

Using the calibrated on-machine system, different roughness gauges corresponding to face and cylindrical milling were digitized. Then, parameters Ra and Rz were calculated from the point clouds gathered on each roughness gauge and compared to those provided by the gauges' manufacturer, which were considered as reference values. As stated in roughness standards referred to contact profilometers, this analysis also required to apply a double filtering process to remove waviness and high frequency noise coupled to the roughness profiles. An adaptation of the high frequency filtering procedure had to be developed to consider the influence on the measurement accuracy of factors associated to the laser spot (e.g., size and asymmetrical shape) as well as the optical behaviour of the surface. In this sense, a Gaussian-type kernel was applied using a gain parameter k adjusted to provide specific recommendations adapted to the lens used and the characteristics of the surface verified (e.g., roughness grades or type of milling process).

In the case of face milling, results revealed that it was not necessary to apply the high frequency filter to verify the values of parameter Ra from N8 to N10 roughness grades nor for the values of parameter Rz from N9 and N10. With respect to the rest of grades, different values of the gain parameter k should be used to meet similar values of Ra and Rz provided by the roughness gauges' manufacturer.

A similar situation was observed in cylindrical milling although in this case, the parameter Ra only required a high frequency filter for grades N5, N6 and N8, whereas Rz also included grade N7.

In practice, when verifying the roughness of a surface machined by these processes using the CH system integrated in the MC, the following procedure shall be used:

1) Digitize a profile of the analysed surface to determine the RSm, and then adjust the value of λ_c following ISO 4288 [47].
2) According to the roughness specification expressed in the part drawing or to the expected surface roughness grade (e.g., derived from haptic comparison or process parameters), determine the values of k recommended in this work (tables 6 and 7) and, therefore, the corresponding values of λ_s (Eq. 11).
3) Process the profile using these filtering configurations to obtain the value of the parameters Ra and Rz.
4) If the values of Ra and Rz do not match the expected ones, the surface is out of specification, unless the value of RSm was not well determined initially. In the latter case, repeat the procedure with a new value of RSm.

As a final conclusion, it can be stated that the CH system integrated in the machining centre was demonstrated as an effective non-contact technology able to provide reliable roughness measurements in industrial milling processes.

References

[1] Palani S, Natarajan U. Prediction of surface roughness in CNC end milling by machine vision system using artificial neural network based on 2D Fourier transform. Int J Adv Manuf Tech 2011; 54: 1033–1042.

[2] Quinsat Y, Tournier C. In situ non-contact measurements of surface roughness.

Precis Eng 2012; 36: 97–103.

[3] Mahashar Ali J, Siddhi Jailani H, Murugan M. (2019) Surface Roughness Evaluation of Milled Surfaces by Image Processing of Speckle and White-Light Images. In: Advances in Manufacturing Processes, London, UK 2019. p. 141–151.

[4] Poon CY, Bhushan B. Comparison of surface roughness measurements by stylus profiler, AFM and non-contact optical profiler. Wear 1995; 190: 76–88.

[5] Patel DR, Kiran MB. A non-contact approach for surface roughness prediction in CNC turning using a linear regression model. Mater Today-Proc 2020; 26: 350–355.

[6] Hayajneh MT, Tahat MS, Bluhm J. (2007). A study of the effects of machining parameters on the surface roughness in the end-milling process. Jordan Journal of Mechanical and Industrial Engineering 2007; 1: 1–5.

[7] ISO 4287, 1997. Geometrical Product Specifications (GPS) – Surface Texture: Profile Method – Terms, Definitions and Surface Texture Parameters.

[8] Samtaş G. Measurement and evaluation of surface roughness based on optic system using image processing and artificial neural network. Int J Adv Manuf Tech 2014; 73: 353–364.

[9] Lee DH, Cho NG. Assessment of surface profile data acquired by a stylus profilometer. Meas Sc Technol 2012; 23: 105601.

[10] Hoy, DEP, Yu, F. Surface quality assessment using computer vision methods. J Mat Process Tech 1991; 28: 265–274.

[11] Dhanasekar B, Ramamoorthy B. Assessment of surface roughness based on super resolution reconstruction algorithm. Int J Adv Manuf Tech 2008; 35: 1191–1205.

[12] Hocken RJ, Chakraborty N, Brown C. Optical metrology of surfaces. Cirp Ann-

Manuf Techn 2005; 54: 169–183.

[13] Schwenke H, Neuschaefer-Rube U, Pfeifer T, Kunzmann H. Optical methods for dimensional metrology in production engineering. Cirp Ann-Manuf Techn 2002; 51: 685–699.

[14] Xu X, Hu H. Development of non-contact surface roughness measurement in last decades. In: Proc. IEEE International Conference on Measuring Technology and Mechatronics Automation 2009. p. 210–213.

[15] Hu Y, Chen Q, Feng S, Zou C. Microscopic fringe projection profilometry: A review. Opt Laser Eng 2020; 135: 106192.

[16] Feng P, Borghesani P, Smith WA, Peng Z. Model-based surface roughness estimation using acoustic emission signals. Tribol Int 2020; 144: 106101.

[17] Zou Y, Li Y, Kaestner M, Reithmeier E. Low-coherence interferometry based roughness measurement on turbine blade surfaces using wavelet analysis. Opt Laser Eng 2016; 82: 113–121.

[18] Shahabi HH, Ratnam MM. Noncontact roughness measurement of turned parts using machine vision. Int J Adv Manuf Tech 2010; 46: 275–284.

[19] He W, Zhong K, Li Z, Meng X, Cheng X, Liu X, Shi Y. Accurate calibration method for blade 3D shape metrology system integrated by fringe projection profilometry and conoscopic holography. Opt Laser Eng 2018; 110: 253–261.

[20] Minoni U, Cavalli F. Surface quality control device for on-line applications. Measurement 2008; 41: 774–782.

[21] Vithin AVS, Show I, Ajithaprasad S, Gannavarpu R, Rajshekhar G. Demodulating interferograms with non-uniform amplitude variations for precision non-contact

optical profilometry. Opt Laser Eng 2020; 134: 106292.

[22] Frade M, Enguita JM, Álvarez I. In situ 3D profilometry of rough objects with a lateral shearing interferometry range finder. Opt Laser Eng 2012; 50: 1559–1567.

[23] Lim HS, Son SM, Wong YS, Rahman M. Development and evaluation of an on-machine optical measurement device. Int J Mach Tool Manu 2007; 47: 1556–1562.

[24] Li B, Li F, Liu H, Cai H, Mao X, Peng F. A measurement strategy and an error-compensation model for the on-machine laser measurement of large-scale free-form surfaces. Meas Sc Technol 2013; 25: 015204.

[25] Xie Z, Wang X, Chi S. Simultaneous calibration of the intrinsic and extrinsic parameters of structured-light sensors. Opt Laser Eng 2014; 58: 9–18.

[26] Yin Z, Li S, Tian F. Exact reconstruction method for on-machine measurement of profile. Precis Eng 2014; 38: 969–978.

[27] Pagliarulo V, Farroni F, Ferraro P, Lanzotti A, Martorelli M, Memmolo P, Speranza D, Timpone F. Combining ESPI with laser scanning for 3D characterization of racing tyres sections. Opt Laser Eng 2018; 104: 71–77.

[28] Van Gestel N, Cuypers S, Bleys P, Kruth JP. A performance evaluation test for laser line scanners on CMMs. Opt Laser Eng 2009; 47: 336–342.

[29] Isheil A, Gonnet JP, Joannic D, Fontaine JF. Systematic error correction of a 3D laser scanning measurement device. Opt Laser Eng 2011; 49: 16–24.

[30] Muralikrishnan B, Ren W, Everett D, Stanfield E, Doiron T. Performance evaluation experiments on a laser spot triangulation probe. Measurement 2012; 45: 333–343.

[31] Vukašinović N, Možina J, Duhovnik J. Correlation between incident angle, measurement distance, object colour and the number of acquired points at CNC laser

scanning. Stroj Vestn-J Mech E 2012; 58: 23–28.

[32] Sirat G, Psaltis D. Conoscopic holography. Opt Lett 1985; 10: 4–6.

[33] Malet Y, Sirat GY. Conoscopic holography application: multipurpose rangefinders. J Opt UK 1998; 29: 183–187.

[34] Galantucci LM, Lavecchia F, Percoco G. Experimental study aiming to enhance the surface finish of fused deposition modeled parts. Cirp Annals 2009; 58: 189–192.

[35] Zhu L, Barhak J, Srivatsan V, Katz R. Efficient registration for precision inspection of free-form surfaces. Int J Adv Manuf Tech 2007; 32: 505–515.

[36] Hong E, Zhang H, Katz R, Agapiou JS. Non-contact inspection of internal threads of machined parts. Int J Adv Manuf Tech 2012; 62: 221–229.

[37] Zapico P, Patiño H, Valiño G, Fernández P, Rico JC. CNC centralized control for digitizing freeform surfaces by means of a conoscopic holography sensor integrated in a machining centre. Precis Eng 2019; 55: 474–483.

[38] Gaburro N, Marchioro G, Daffara C. A versatile optical profilometer based on conoscopic holography sensors for acquisition of specular and diffusive surfaces in artworks. In: Pezzati L, Targowski P. editors: Optics for Arts, Architecture, and Archaeology VI, Munich, Germany, 2017. SPIE: International Society for Optics and Photonics, 2017. 10331 103310A.

[39] Brudfors M, García- Vázquez V, Sesé- Lucio B, Marinetto E, Desco M, Pascau J. ConoSurf: Open- source 3D scanning system based on a conoscopic holography device for acquiring surgical surfaces. Int J Med Robot Comp 2016; 13: e1788.

[40] Senin N, Groppetti R, Garofano L, Fratini P, Pierni M. Three- dimensional surface topography acquisition and analysis for firearm identification. J Forensic Sci 2006;

51: 282–295.

[41] Spagnolo GS, Cozzella L, Simonetti C. Linear conoscopic holography as aid for forensic handwriting expert. Optik 2013; 124: 2155–2160.

[42] Optimet.com. Optimet ConoPoint Series, User Manual, Rev. 8; c2018 (Accessed Feb 4 2020). https://www.optimet.com/.

[43] Rico JC, Valiño G, Fernández P, Zapico P, Blanco D, Mateos S. Adjustment recommendations of a conoscopic holography sensor for a reliable scanning of surfaces with roughness grades obtained by different processes. Precis Eng 2015; 42: 335–345.

[44] Sirat GY, Paz F, Agronik G, Wilner K. Conoscopic systems and conoscopic holography. Optimet, Optimet White Paper 2005.

[45] Optimet.com. OEM Manual for OPTIMET'S Mark10/10HD, Rev. 2; c2014 (Accessed Feb. 4 2020). https://www.optimet.com/.

[46] Hamamatsu.com. Opto-semiconductor handbook 2014, Chapter 5 – Image sensors; c2014 (Accessed Feb 4 2020). https://www.hamamatsu-news.de/hamamatsu_optosemiconductor_handbook/.

[47] ISO 4288, 1996. Geometrical product specifications (GPS) – surface texture: profile method – rules and procedures for the assessment of surface texture.

[48] ISO 16610-20, 2015. Geometrical product specifications (GPS) – Filtration – Part 20: Linear profile filters: Basic concepts.

[49] ISO 16610-21, 2011. Geometrical Product Specifications (GPS) – Filtration – Part 21: Linear Profile Filters: Gaussian Filters.

[50] ISO 3274, 1996. Geometrical Product Specifications (GPS) – Surface texture:

Profile method – Nominal characteristics of contact (stylus) instruments.

[51] Patiño H, Zapico P, Rico JC, Fernández P, Valiño G. A Gaussian filtering method to reduce directionality on high-density point clouds digitized by a conoscopic holography sensor. Precis Eng 2018; 54: 91–98.